Int. J. of Refractory Metals & Hard Materials **15** (1997) 341–355
© 1997 Elsevier Science Limited
Printed in Great Britain. All rights reserved
0263-4368/97/$17.00

PII: S0263-4368(96)00014-0

Atomistic Simulation of Σ3 (111) Grain Boundary Fracture in Tungsten Containing Various Impurities

M. Grujicic, H. Zhao

Program in Materials Science and Engineering, Department of Mechanical Engineering, 241 Flour Daniel EIB, Clemson University, Clemson, SC 29631-0921, USA

& G. L. Krasko

US Army Research Laboratory, Materials Directorate, AMSRL-MA-CC, Aberdeen Proving Ground, MD 21005-5096, USA

(Received 14 April 1997; accepted 27 August 1997)

Abstract: The effect of various impurities and micro-alloying additions (B, N, C, O, Al, Si, S and P) on the intrinsic resistance of the Σ3 (111) grain boundary in tungsten has been investigated using the molecular dynamics simulation. The atomic interactions have been accounted for through the use of Finnis–Sinclair interatomic potentials. The fracture resistance of the grain boundary has been characterized by computing, in each case, the ideal work of grain boundary separation, the mode I stress intensity factor and the Eshelby's F_1 conservation integral at the onset of crack propagation. The results obtained suggest that pure tungsten is relatively resistant to grain boundary decohesion and that this resistance is further enhanced by the presence of B, C and N. Elements such as O, Al and Si however, have a relatively minor effect on the cohesion strength of the Σ3 (111) grain boundary. In sharp contrast, S and P greatly reduce this strength making tungsten quite brittle. These findings have been correlated with the effect of the impurity atoms on material evolution at the crack tip. © 1997 Elsevier Science Ltd. All rights reserved

INTRODUCTION

Tungsten–base alloys, due to their high density and strength, are widely used in army systems, especially for anti-armor applications. However, technically pure tungsten is extremely brittle and its ductile→brittle transition temperature (DBTT) is typically as high as 300°C. To overcome the problems associated with the limited toughness of tungsten, the so-called tungsten heavy alloys (THAs) have been developed[1]. Manufactured by liquid phase sintering, these alloys are actually metal–matrix composites consisting of hard tungsten particles embedded in a relatively mild Ni–Fe matrix. Although the density of THAs is only slightly lower than that of pure tungsten, the alloys' anti-armor performance is quite inferior relative to that of depleted uranium, a competing anti-armor material. This difference is related to the fact that, while a depleted uranium penetrator develops adiabatic shear bands upon impact which give rise to a 'self-sharpening' effect[2], the THA penetrators 'mushroom', which leads to an increase in the penetrator diameter and, in turn, to a reduction in the depth of penetration. Owing to the well-known environmental problems associated with using depleted uranium, significant resources are currently being directed towards developing THAs with

Report Documentation Page	*Form Approved* *OMB No. 0704-0188*

1. REPORT DATE **1997**	2. REPORT TYPE	3. DATES COVERED **00-00-1997 to 00-00-1997**

4. TITLE AND SUBTITLE **Atomistic Simulation of E3 (111) Grain Boundary Fracture in Tungsten Containing Various Inpurities**	5a. CONTRACT NUMBER
	5b. GRANT NUMBER
	5c. PROGRAM ELEMENT NUMBER
6. AUTHOR(S)	5d. PROJECT NUMBER
	5e. TASK NUMBER
	5f. WORK UNIT NUMBER
7. PERFORMING ORGANIZATION NAME(S) AND ADDRESS(ES) **Celmson University,Department of Mechanical Engineering,Clemson,SC,29634**	8. PERFORMING ORGANIZATION REPORT NUMBER
9. SPONSORING/MONITORING AGENCY NAME(S) AND ADDRESS(ES)	10. SPONSOR/MONITOR’S ACRONYM(S)
	11. SPONSOR/MONITOR’S REPORT NUMBER(S)

12. DISTRIBUTION/AVAILABILITY STATEMENT

Approved for public release; distribution unlimited

13. SUPPLEMENTARY NOTES

14. ABSTRACT

The effect of various impurities and micro-alloying additions (B, N, C 0, AI, Si, S and P) on the intrinsic resistance of the ~3 (111) grain boundary in tungsten has been investigated using the molecular dynamics simulation. The atomic interactions have been accounted for through the use of Finnis-Sinclair interatomic potentials. The fracture resistance of the grain boundary has been characterized by computing, in each case, the ideal work of grain boundary separation, the mode I stress intensity factor and the Eshelby’s F, conservation integral at the onset of crack propagation. The results obtained suggest that pure tungsten is relatively resistant to grain boundary decohesion and that this resistance is further enhanced by the presence of B, C and N. Elements such as 0, AI and Si however, have a relatively minor effect on the cohesion strength of the ~3 (111) grain boundary. In sharp contrast, S and P greatly reduce this strength making tungsten quite brittle. These findings have been correlated with the effect of the impurity atoms on material evolution at the crack tip.

15. SUBJECT TERMS

16. SECURITY CLASSIFICATION OF:			17. LIMITATION OF ABSTRACT	18. NUMBER OF PAGES	19a. NAME OF RESPONSIBLE PERSON
a. REPORT **unclassified**	b. ABSTRACT **unclassified**	c. THIS PAGE **unclassified**	**Same as Report (SAR)**	**15**	

improved adiabatic shear band behavior. The usual approach is to significantly modify, or find an alternative to, the Ni–Fe matrix.

A different approach has recently been initiated by Krasko[3], who suggested micro-alloying as a way of obtaining a 'ductile' tungsten. Being a B.C.C. metal, such tungsten is expected to acquire the necessary adiabatic shear band behavior since the latter has already been observed in high-strength B.C.C. steels in conditions of 'marginal' ductility[4].

The reduced cohesion of grain boundaries is frequently cited as a major factor limiting ductility and, in turn, the performance and reliability of high-strength metallic materials[5,6]. Intergranular embrittlement in metals is usually caused by impurities segregating to the grain boundaries. Impurities present in bulk concentrations of only 10–100 parts per million (ppm) can result in a dramatic decrease in the mechanical properties (primarily ductility, fracture toughness and fracture strength) of metallic materials, and thus pose significant processing and application problems. This detrimental effect of mere ppm amounts of impurities is consistent with the fact that only few ppms of impurities are sufficient to saturate all the grain boundaries in a polycrystal of the typical grain-size (10–100 μm)[3]. The sensitivity of DBTT to the grain size confirms the aforementioned effect of grain boundary impurities. That is, the smaller the grain size, the larger the amount of impurities required to saturate the grain boundaries at a given temperature and hence, at the same bulk concentration of impurities, the higher toughness levels and the lower DB — TT are expected in fine-grained polycrystals.

In addition to the smaller grain size, increasing the purity of the metallic system, in general, increases the material's ductility and lowers its DBTT. For example, the DBTT in high purity W single crystals processed by electron-beam zone remelting, involving the use of a special impurity gettering procedure, was found to be as low as −196°C. If impurities are the main cause of embrittlement in tungsten, gettering the impurities is the obvious way of ductilizing this metal. A well-known, though extremely expensive, purity enhanced procedure is the so-called 'rhenium effect'[7,8]. While the actual mechanism of the rhenium effect is not yet completely understood, it is believed to be based on the gettering of oxygen[7,8]. A more promising way of removing 'harmful' impurities, such as O, N, P, etc., from the grain boundary is by gettering them with micro-alloying additions of selected elements, e.g. boron, which leads to the formation of compounds such as boron oxides, boron nitrides, etc.[9–11]. This process, however, requires a careful control of the material chemistry since ductility improvements due to impurity gettering can be expected only so far as the resulting compound precipitates are fine. The coagulation and coarsening of the precipitates generally result in an adverse embrittling effect.

using both semi-empirical and first-principles calculations, Krasko[3] carried out a theoretical analysis of clean tungsten grain boundaries and grain boundaries containing various impurities. His work provided some important results regarding the effect of various grain boundary impurities and micro-alloying additions. For instance, impurities such as H, N, O, P, S, Si are found to weaken the intergranular cohesion in tungsten. On the contrary, the presence of B and C was found to enhance the bonding across the grain boundary, thus improving the intergranular cohesion. Furthermore, the so-called site-competition effect, as a result of which the species with a lower energy at the grain boundary tend to replace the species which have a higher energy at the grain boundary, was found to play an important role in affecting the impurity distribution at the tungsten grain boundaries[3]. Among the atomic species analyzed, B was found to have the lowest energy at the grain boundary, and thus wound tend to displace other impurity atoms from the grain boundary, while at the same time enhancing the intergranular cohesion. Based on these findings, micro-alloying of technically pure tungsten with 10–50 ppm of B was recommended as a way of enhancing the ductility of this metal[3]. Experimental investigation of tungsten alloyed with B in amounts 15 times higher than the one recommended by Krasko[3] was found to result in a significant (150°C) drop in the DBTT[9–11]. Microstructural analysis further revealed the presence of relatively coarse boron oxide particles which are the result of the excessive amount of B in the tungsten. This suggests that the addition of 10–50 ppm of B which is sufficient to completely displace oxygen from the grain boundaries via the 'site competition' effect without an excessive formation of boron oxide, as suggested by Krasko, may result in even higher levels of ductility and fracture toughness.

In the present work, the molecular dynamics method was used to explore the effect of impurities and micro-alloying additions (B, C, N, O, Al, S, Si, P) on the fracture resistance of the Σ3 (111) grain boundary in tungsten. The organization of the paper is as follows. Modifications of the 'environment sensitive embedding' (ESE) energy functions for various grain boundary impurities in tungsten are discussed below. Generation of the computational crystal containing a crack along the Σ3 (111) grain boundary is presented in the section 'Computational crystal'. Computations of the ideal work of grain boundary separation and the F_1 conservation integral are discussed in the next two sections, respectively. The section 'Results and Discussion' contains the results obtained in the present study, while the main conclusions are drawn in the final section.

PROCEDURE

Modification of the Finnis–Sinclair functions for tungsten

Within the EAM formalism[12,13] the total potential energy of the system is given as the sum of two energy contributions, the interaction of each atom with the local electron density associated with the remaining atoms in the system, called the embedded energy, and a pair-wise interaction term reflecting the electrostatic interactions between the atoms. In particular, the total potential energy is written as:

$$E_{\mathrm{tot}} = \sum_i F_i(\rho_i) + \frac{1}{2} \sum_{i,j,i \neq j} \phi_{i,j}(R_{i,j}) \tag{1}$$

where, F_i is the embedded energy of atom i, ρ_i is the electron density at atom i, and $\phi_{ij}(R_{ij})$ is the pair-wise interaction between atoms i and j separated by the distance R_{ij}. The electron density at each site is computed from the superposition of spherically averaged atomic electron densities as:

$$\rho_i = \sum_{j \neq i} \rho_j^{\alpha}(R_{i,j}) \tag{2}$$

$\rho_j^{\alpha}(R_{ij})$ in eqn (2) represents the atomic electron density at site i due to an atom at site j at a distance R_{ij}. The superscript α in $\rho_j^{\alpha}(R_{ij})$ is used to specify the species of the atom at site j. The embedding energies and pair-wise interaction functions in eqn (1) are generally determined by fitting various physical quantities of the material such as the sublimation energy, the equilibrium lattice parameters, the second-order elastic constants, the various defect formation energies and the zero-temperature equation of state[14].

The Finnis–Sinclair method[15] that is usually called 'the N-body potential approach' has a slightly different foundation, but the total potential energy can be still expressed in the form of eqn (1). The first term, however, has a different meaning since it originates from the tight-binding theory according to which:

$$F(\rho_i) = -A\sqrt{\rho_i} \tag{3}$$

where A is a species-dependent parameter whose value for tungsten (1·896373 eV) was determined by Finnis and Sinclair[15] and ρ_i now represents an environment-dependent effective atomic coordination number, or an effective atomic density at site i. Finnis and Sinclair[15] originally proposed the following functional form for ρ_i:

$$\begin{aligned} \rho_i^{\mathrm{h}}(R_{i,j}) &= (R_{i,j} - R_{\mathrm{cut}})^2, && \text{for } R_{i,j} \leq R_{\mathrm{cut}} \\ \rho_i^{\mathrm{h}}(R_{i,j}) &= 0 && \text{for } R_{i,j} > R_{\mathrm{cut}} \end{aligned} \tag{4}$$

where the superscript h stands for 'host atoms'. For tungsten, Finnis and Sinclair set the cut-off distance R_{cut} to a value 4·400224 Å.Finnis and Sinclair[15] further proposed the following form for the pair-wise potential function ϕ_{ij}:

$$\phi_{i,j}(R_{i,j}) = (R_{i,j} - c)^2(c_0 + c_1 R_{i,j} + c_2 R_{i,j}^2), \quad \text{for } R_{i,j} \leq c$$

and

$$\rho_{i,j}(R_{i,j}) = 0 \quad \text{for } R_{i,j} > c \tag{5}$$

where, for tungsten, the cut-off distance c is set to a value 3·4 Å, and the quadratic polynomial coefficients are $c_0 = 47{\cdot}13465$, $c_1 = -33{\cdot}7665655$, and $c_2 = 6{\cdot}254199$.For tungsten containing interstitial impurities, Krasko[3] introduced a modified Finnis–Sinclair formulation by simply adding a term to eqn (1) to account for the energy of impurity atoms in the host environment. The modified E_{tot} is then written as:

$$E_{\mathrm{tot}} = \sum_i F(\rho_i^{\mathrm{h}}) + \frac{1}{2} \sum_{i,j} \phi_{i,j}(R_{i,j}) + \sum_k ESE(\rho_k^{\mathrm{imp}}) \tag{6}$$

where first two terms on the right-hand side of eqn (6) are given by eqns (3)–(5), while the third term represents the sum of the 'environment-sensitive embedding' (ESE) energies of the impurity atoms, and is equal to the interaction energy between the impurity and host atoms, ρ_k^{imp} is the electron density at the site of impurity atom k due to the surrounding host atoms, and is given as:

$$\rho_k^{\text{imp}} = \sum_j \rho_k^{\text{H}} = \sum_j \rho_j^{\text{H}}(R_{kj}) \qquad (7)$$

where $\rho_j^{\text{H}}(R_{ij})$ represents the electron density defined by eqn (4) at the site k of an impurity atom due to the host atom at site j, while R_{kj} is the distances between the impurity atom at site k and a host atom at site j.As mentioned above the *ESE* functions introduced by Krasko[3] were derived in the spirit of EAM, that is relative to the free atom electron density at the impurity site due to the host atoms, ρ_j^{H}, while the host atom embedded function are expressed relative to the effective atomic density, ρ_i^{h}. To avoid possible confusion relative to the meaning of the density functions used, the ESE functions were rederived in the present paper relative to the effective atomic density used by Finnis and Sinclair, ρ_i^{h}. The resulting $ESE(\rho^{\text{imp}})$ expressed as fourth-order polynomials are given as:

$$ESE(\rho^{\text{imp}}) = \rho^{imp}(C_0 + C_1\rho^{\text{imp}} + C_2(\rho^{\text{imp}})^2 + C_3(\rho^{\text{imp}})^3 \qquad (8)$$

The values of the coefficients C_0, C_1, C_2 and C_3 for various impurities and micro-alloying additions are given in Table 1 and the corresponding *ESO* vs ρ^{imp} functions are plotted in Fig. 1.

Table 1. Environment-sensitive embedded energy, *ESE*, vs effective atomic density, ρ, function coefficients for various impurities in tungsten

$ESE(\text{eV}) = \rho(C_0+C_1\rho+C_2\rho^2+C_3\rho^3)$				
Impurity	C_0	C_1	C_2	C_3
B	−0·8926	0·0099	$-2{\cdot}548\times10^{-5}$	$7{\cdot}833\times10^{-9}$
C	−0·6177	0·0125	$-6{\cdot}223\times10^{-5}$	$1{\cdot}124\times10^{-7}$
N	−0·9423	0·0157	$-6{\cdot}222\times10^{-5}$	$7{\cdot}834\times10^{-8}$
O	−0·6202	0·0134	$-4{\cdot}798\times10^{-5}$	$5{\cdot}044\times10^{-8}$
Al	−0·6259	0·0244	$-8{\cdot}997\times10^{-5}$	$9{\cdot}926\times10^{-8}$
Si	−0·5201	0·0233	$-8{\cdot}199\times10^{-5}$	$8{\cdot}131\times10^{-8}$
S	−0·1674	0·0224	$-8{\cdot}132\times10^{-5}$	$8{\cdot}522\times10^{-8}$
P	−0·3655	0·0299	$-1{\cdot}292\times10^{-4}$	$1{\cdot}792\times10^{-7}$

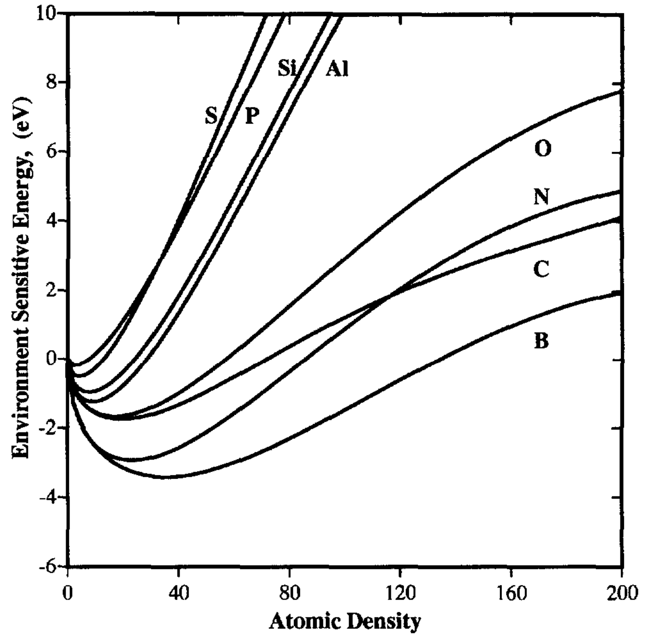

Fig. 1. Environment sensitive embedding (*ESE*) energy vs atomic electron density functions for various grain-boundary impurities and micro-alloying additions in tungsten.

Computational crystal

Generation of the grain boundary

simulations were carried out using a cylindrical crystal whose crystallographic orientation is shown in Fig. 2. The dimensions of the crystal are given in terms of the number of $(\bar{1}\bar{1}2)$, (111), $(\bar{1}10)$ B.C.C. interplanar spacings along the three principal axes. The initial diameter of the crystal was approximately 9 nm.

To generate a Σ3 (111) grain boundary, the atoms in the upper part of the computational crystal ($x_2 > 0$) were rearranged to produce a configuration which is a mirror image of the

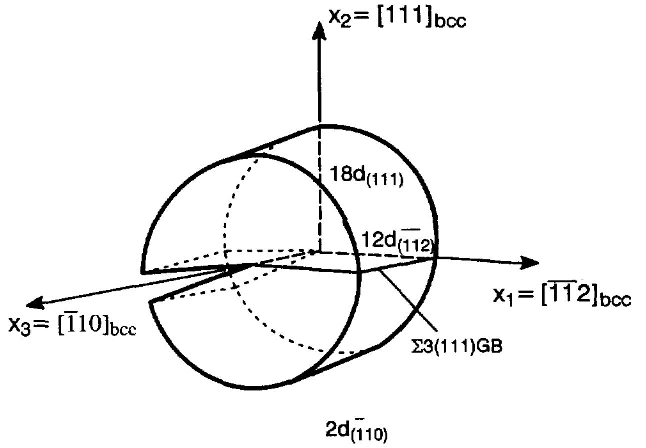

Fig. 2. Schematic, size and the crystallographic orientation of the computational crystal used in the present work.

lower part of the crystal across the grain boundary plane ($x_2 = 0$). The resulting structure of the computational crystal can be represented by succession of the (111) B.C.C. planes as:

$$C\ B\ A\ C\ B\ A\ C\ B\ \mathcal{A}\ B\ C\ A\ B\ C\ A\ B\ C \qquad (8)$$

where the grain boundary is marked by $\mathcal{A}$. This grain boundary is of a tilt type and is characterized by an inverse coincidence lattice number $\Sigma = 3$. Krasko[3] showed that, due to the associated lowest energy level, an impurity atom such as B, C, N, etc., is most likely to occupy an interstitial position in the center of the trigonal prism formed by 6 W atoms in the Σ3 (111) grain boundary. Consequently, all the simulations of the Σ2 (111) grain boundary containing impurities were done under the condition that the impurity atoms occupy the interstitial sites associated with the trigonal prisms along the grain boundary plane. It should be noted that for a typical grain size range of 10–100 μm, the introduction of interstitials into every grain boundary interstitial site corresponds to the impurity concentration range of 80–20 ppm.

Grain boundary crack

To generate a crack along the Σ3 (111) grain boundary, all the atoms in the computational crystal were displaced from their initial positions in accordance with the plane strain linear elastic solution developed by Sih and Liebowitz[16] for the crack displacements in an anisotropic single crystal. While, in general, the single-crystal solution of Sih and Liebowitz[16] is not valid for interfacial cracks, the fact that the two crystals in Fig. 2 had identical corresponding crystallographic directions in the three principal directions, justifies the use of this plane procedure. Under a pure tensile load applied in the x_2 direction and for plane strain condition along the x_3 direction the components of the displacement along the three principal axes are given as following:

$$u_1 = K_{\rm I}\sqrt{\frac{2r}{\pi}}\, Re\left\{\frac{1}{S_1 - S_2}\right.\times[s_1 p_2(\cos\theta + s_2 \sin\theta)^{1/2}$$
$$\left. - s_2 p_1(\cos\theta + s_1 \sin\theta)^{1/2}]\right\}$$

$$u_2 = K_{\rm I}\sqrt{\frac{2r}{\pi}}\, Re\left\{\frac{1}{S_1 - S_2}\right.\times[s_1 q_2(\cos\theta + s_2 \sin\theta)^{1/2}$$
$$\left. - s_2 q_1(\cos\theta + s_1 \sin\theta)^{1/2}]\right\}$$

$$u_3 = 0 \qquad (9)$$

where r and θ are the polar coordinates, i.e. the radial distance and the angle between the radial line and the x_1-axis in Fig. 2. Functions p_j and $q_j (j = 1,2)$ are defined as:

$$p_1 = a_{11}s_1^2 + a_{12} - a_{16}s_1$$
$$p_2 = a_{11}s_2^2 + a_{12} - a_{16}s_2$$
$$q_1 = \frac{a_{12}s_1^2 + a_{22} - a_{26}s_1}{s_1}$$
$$q_2 = \frac{a_{12}s_2^2 + a_{22} - a_{26}s_2}{s_2} \qquad (10)$$

where $s_1 = \mu_1\alpha_1 + i\beta_1$ and $s_2 = \mu_2 = \alpha_2 + i\beta_2$ are two non-complex conjugate roots of the following characteristic equation:

$$a_{11}\mu_j^4 - 2a_{16}\mu_j^3 + (2a_{12} + a_{66})\mu_j^2 - 2a_{26}\mu_j + a_{22} = 0 \qquad (11)$$

The remaining two solutions of eqn (11) are the corresponding complex conjugates of the first two, ie $\mu_3 = \mu^*_1$ and $\mu_4 = \mu^*_2$. a_{ij} coefficients appearing in eqns (10) and (11) are related to the elastic compliance constants of the material, S_{ij}, and for plane-strain are given as:

$$a_{11} = \frac{S_{11}S_{33} - S_{13}^2}{S_{33}}, \quad a_{12} = a_{21} = \frac{S_{12}S_{33} - S_{13}S_{23}}{S_{33}}$$
$$a_{22} = \frac{S_{22}S_{33} - S_{23}^2}{S_{33}}, \quad a_{16} = a_{61} = \frac{S_{16}S_{33} - S_{13}S_{36}}{S_{33}}$$
$$a_{66} = \frac{S_{66}S_{33} - S_{36}^2}{S_{33}}, \quad a_{26} = a_{62} = \frac{S_{26}S_{33} - S_{13}S_{36}}{S_{33}} \qquad (12)$$

For a given material, the elastic compliance constants used in eqn (12) depend on the crystallographic orientation of the computational crystal being examined. Parameter $K_{\rm I}$ appearing in eqn (9) is the mode I stress intensity factor whose critical value associated with the reversible crack extension, the Griffith stress intensity factor, $K_{\rm Gr}$, is given as[16]:

$$K_{\mathrm{Gr}} = \sqrt{2\gamma_{\mathrm{sep}}/A} \qquad (13)$$

where A is defined as:

$$A = \left\{\left(\frac{a_{11}a_{22}}{2}\right)\left[\left(\frac{a_{22}}{a_{11}}\right)^{1/2} + \frac{2a_{12}+a_{66}}{2a_{11}}\right]\right\}^{1/2} \qquad (14)$$

and this parameter also in the relationship between the J_{I}-integral and the stress intensity factor K_{I}, $J_{\mathrm{I}} = AK_{\mathrm{I}}^2$ [eg [16]].The $2\gamma_{\mathrm{sep}}$ term appearing in eqn (13) represents the ideal work of grain boundary separation and is equal to the amount by which the work per unit area of the crack surface done by the external loads exceeds the change in the elastic strain energy. At the onset of crack growth, $2\gamma_{\mathrm{sep}}$ is given as:

$$2\gamma_{sep} = \gamma_s^A + \gamma_s^B - \gamma_{int}^{A/B} \qquad (15)$$

where superscripts A and B denote the two crystals being jointed along the grain boundary, γ_{s} is the surface energy and γ_{int} the grain boundary (interface) energy.

Computation of the ideal work of grain boundary separation, $2\gamma_{\mathrm{int}}$

To compute the surface energy associated with the $(111)_{\mathrm{bcc}}$ crystallographic plane, the crack plane, a rectangular slab with the same orientation as the computational crystal shown in Fig. 2 and with its top and bottom surfaces parallel to this plane is created. The height of the crystal is chosen to be large enough to avoid the interaction between the top and the bottom surfaces. With the periodic boundary conditions applied in the other two orthogonal directions, the energy of the slab is minimized. The surface energy is then defined as the excess energy per unit surface area of this crystal, relative to the one of the same size in which the periodic boundary conditions are applied in all three directions.

The above procedure is repeated using a slab containing the Σ3 (111) grain boundary and the corresponding grain boundary energy calculated as the excess energy of the slab per unit grain boundary area relative to the perfect B.C.C. without a grain boundary subject to the periodic boundary condition in all the direction.

The same procedure for calculating the surface and the grain boundary energy was utilized for the cases where the initial grain boundary contains one of the impurities or micro-alloying additions. The results of the above procedure for pure tungsten and tungsten containing impurities are summarized in Table 2.

Table 2. $(111)_{\mathrm{bcc}}$ surface energy, γ_{surf}, Σ3 $(111)_{\mathrm{bcc}}$ grain boundary energy, γ_{GB}, and the corresponding ideal work of grain boundary decohesion, $2\gamma_{\mathrm{int}}$, for tungsten containing various impurities

Impurity	γ_{surg}, (eV/Å^2)	γ_{GB}, (eV/Å^2)	$2\gamma_{\mathrm{int}}$, (eV/Å^2)
pureW	0·4285	0·5823	0·2747
B	0·3006	0·0909	0·6382
C	0·3007	0·1216	0·6076
N	0·2583	0·0943	0·5925
O	0·2135	0·3290	0·3130
Al	0·1746	0·3263	0·2768
Si	0·1925	0·3074	0·3136
S	0·0735	0·3515	0·1505
P	0·1100	0·3275	0·2110

Molecular dynamics method

The evolution of the material surrounding the crack tip is studied using the standard molecular dynamics procedure at 100 K. The molecular dynamics calculations involve the solution of the Newton equations of motion for a system of interacting particles (atoms) in order to determine the classical particles trajectories and velocities.

At the beginning of each simulation run, a crack was generated by displacing all atoms according to eqn (9) from their initial positions corresponding to the perfect unrelaxed B.C.C. bicrystal structure shown in Fig. 2. All the molecular dynamics simulation runs were done under the fixed periodic boundary conditions in the $x_3 = [110]_{\mathrm{bcc}}$ direction to ensure the plane strain condition in this direction. Also, at each level of K_{I}, fixed displacement boundary conditions were applied onto the outer surface of the computational crystal.

The temperature at which all the simulation runs were carried out, 100 K, was set by initially assigning to each atom a random velocity according to the Boltzmann distribution. During the simulatino process, the temperature was maintained constant by exponentially relaxing, at each time step (2 fs), the average squared atomic velocity using a time constant of 0·1 ps. Using this procedure, the temperature could be maintained within 3% of its target value.

Computation of $\mathbf{F}_1$ integral

To quantify the effect of the crack-tip stress relaxation processes on the resistance of a $\Sigma 3$ (111) grain boundary to separation, the Eshelby's conservation **F** integral[17] was calculated for both the pure tungsten case and the cases of tungsten containing one of the impurities or micro-alloying additions. The **F** integral provides a means for determination of the energy release rate accompanying the crack extension in cases where material nonlinearity effects cannot be neglected. **F** is a vector and its components along the three principal axes (the cracking direction x_1, the crack plane normal direction x_2 and the crack front direction x_3) represent the three force components acting on the crack tip. For the computational crystal and the crack orientation used in the present work (Fig. 2), $\mathbf{F}_1$ acts to propagate the crack tip, while $\mathbf{F}_2$ and $\mathbf{F}_3$ are not physical. the components of **F** can be defined using a closed contour Γ which surrounds the crack tip as following:[17]

$$\mathbf{F}_i = \int_\Gamma \left[W\gamma_{ij} - \sigma_{kj}\frac{\partial u_k}{\partial x_i} \right] \mathrm{d}S_j \qquad (16)$$

where W is the strain energy density, $u_k(x_i)$ is the k-component (k = 1,2,3) of the displacement at a point represented by the coordinates $x_i (i = 1,2,3)$, σ_{ij} are the stress components and $\mathrm{d}S_j = \mathrm{d}S{\cdot}n_j$ where n_j is the j component (j = 1,2,3) of the unit outward normal vector to the contour segment of length dS.To calculate the stresses, the procedure proposed by Hoagland *et al.*[18] was used. According to this procedure the strain energy density associated with an atom at the position x_i is defined as:

$$W(x_i) = \frac{E(x_i) - E_0}{\Omega_0} \qquad (17)$$

where $E(x_i)$ is the potential energy of the atom with the coordinates $x_i (i = 1,2,3)$, E_0 is the equilibrium energy which the atom would have in a perfect, stress-free bulk crystal and Ω_0 is the equilibrium atomic volume. The energies $E(x_i)$ and E_0 are calculated using the Finnis–Sinclair interatomic potentials and an energy expression for the potential per atom analogous to eqn (1).Assuming that for small strain increments the strain energy density can be approximated as being quadratic in incremental strains, the stresses are calculated using the following central difference formula:

$$\sigma_{ij} = \frac{\partial W}{\partial \epsilon_{ij}} = \frac{W(x_i + \delta_i) - W(x_i - \delta_i)}{2\Delta u_{ij}} \qquad (18)$$

where ϵ_{ij} are the components of the strain tensor, $\delta_i = u_{ij}x_j$ is a small perturbation of the atomic position which is the result of the application of a small uniform displacement gradient Δu_{ij} to the entire crystal. The value of $\Delta u_{ij} = 0{\cdot}0005$ was found to be optimal in the present work. To compute the components of the stress, one of the Δu_{ij} is set to 0·0005 at a time (the other δu_{ij} are kept at zero), and corresponding nonzero δ_i computed and used in eqn (18).

From the theory of elasticity it is known that the distortions $u_{ij} = \partial u_i / \partial x_j$ are composed of strain (ϵ_{ij}) and rotational (w_{ij}) components, i.e. $u_{ij} = \epsilon_{ij} + w_{ij}$. A strain ellipsoid that relates the extensional strain between an atom and its α-th neighbor: $\epsilon^\alpha = (r^\alpha) - 1$, where r^α and R^α are respectively the atomic distances after and before straining, can be used to obtain the local strain components ϵ_{ij} as following:

$$\epsilon^\alpha = l_i^\alpha l_j^\alpha \epsilon_{ij} \qquad (19)$$

where l_i^α are the directional cosines (in the unstrained lattice) to α atom. eqn (19) simply represents a transformation of the strain components from the coordinate system given in Fig. 2, to the one whose x_1 axis is along the line connecting the two atoms in question, i.e. the atom at whose location the strain components are being evaluated and its α-neighbor. To find the strain components ϵ_{ij} at the position of an atom at least-squares procedure was used to minimize the following sum over the n neighbors of each atom:

$$L_\epsilon = \sum_{\alpha=1}^{n} (\epsilon^\alpha - l_i^\alpha l_j^\alpha \epsilon_{ij})^2 \qquad (20)$$

The minimization procedure $\partial L_\epsilon / \partial \epsilon_{ij} = 0$, yields six linear algebraic (normal) equations which were readily solved using the gauss elimination method (e.g. [19]). The basis for determination of rigid body rotations, w_{ij}, at a particular site is obtained by proceeding in a manner similar to the one employed for the strains. The relationship between displacements of the nearest neighbors from the given atom, u_i^α, and the antisymmetric matrix of the local rotations suggests that the following sum should be minimized:

$$L_{\mathrm{R}}=\sum_{\alpha}[(u_1^{\alpha}+w_{12}x_2^{\alpha}-w_{13}x_3^{\alpha})^2+(u_2^{\alpha}-w_{12}x_1^{\alpha}+w_{23}x_3^{\alpha})^2+(u_3^{\alpha}+w_{13}x_1^{\alpha}-w_{23}x_2^{\alpha})^2] \tag{21}$$

The minimization procedure $\partial L_{\mathrm{R}}/\partial w_{ij}=0$ yields three normal equations which were also readily solved using the gauss elimination method.The evaluation of the $\mathbf{F}_{\mathrm{I}}$ integral given by eqn (16) was done numerically in the present work using the trapezoidal rule[19] along a circular contour around the crack. Owing to the discrete nature of the crystal, all the atoms within a distance of 0·2 nm from the contour were assumed to be associated with the contour. The magnitude of the contour segment dS^{α} corresponding to an atom α is calculated as $dS^{\alpha}=R(\theta_{\alpha+1}-\theta_{\alpha+1})/2$ where R is the contour radius, and $\theta_{\alpha+1}$ and $\theta_{\alpha-1}$ are, respectively, the polar angles for the atoms in the contour which immediately follow and proceed atom α in the counterclockwise direction. The unit vector normal n^{α} to the contour segment dS^{α} is defined as $n^{\alpha}=\cos\theta_{\alpha}i+\sin\theta_{\alpha}j$, where i and j are the unit vectors in x_1 and x_2 directions, respectively.[20]

It should be noted that the strain energy density W, and hence $\mathbf{F}_{\mathrm{I}}$ each have two contributions: one associated with the strain energy density and the other arising from the work of grain boundary separation. The former contribution to $\mathbf{F}_{\mathrm{I}}$, and J_{I} integral, acts to extend while the latter, $2\gamma_{\mathrm{sep}}$, acts to close the crack. Hence, the following relationship holds:

$$\mathbf{F}_{\mathrm{I}}=J_{\mathrm{I}}-2\gamma_{\mathrm{sep}} \tag{22}$$

RESULTS AND DISCUSSION

Ideal work of grain boundary decohesion

The results of our calculation of the (111) surface energy, Σ3 (111) grain boundary energy and of the corresponding work of grain boundary decohesion are listed in Table 2. The results pertain to the case when, after decohesion, all the impurity atoms remain on one of the crack faces whereas the other crack face is clean of impurities. While the magnitudes of the work of separation takes on different values when the impurities are assumed to divide equally between the two crack surfaces (data not shown), the general findings regarding the effect of various grain boundary impurities on the grain boundary decohesion resistance remain. The results shown in Table 2 indicate that, on the one hand, elements such as B, C and N increase the work of Σ3 (111) grain boundary decohesion. On the other hand, elements such as O, Al and Si have a relatively small effect on this work. Lastly, elements such as P and S act as strong grain boundary embrittlers and reduce this work. These findings are further correlated with the grain boundary energy data shown in Table 2. The grain boundary energy data shown that B, C and N reduce the grain boundary energy the most, while P and S reduce this energy the least. This suggests that B, C and N would, via the site-competition effect, tend to displace P and S from the grain boundary, and in turn, enhance the grain boundary cohesion. In other words, the deleterious embrittling effect of impurities such as P and S in tungsten can be, as previously suggested by Krasko,[3] reduced by using micro-alloying additions of micro-alloying elements such as B, C and N.

Initial atomic configurations

The initial atomic configuration of the Σ3 (111) grain boundary in pure tungsten ('clean' grain boundary) containing a crack at the applied stress intensity factor $K_{\mathrm{app}}=2{\cdot}0\,K_{\mathrm{Gr}}=2{\cdot}7694$ MPa m$^{1/2}$ and the corresponding configurations after relaxation (energy minimization) are shown in Fig. 3(a) and (b), respectively. The energy minimization was carried out using the conjugate gradient method.[21] The structure of the grain boundary ahead of the crack after relaxation can be characterized by analyzing the spacing of the adjacent (111) planes as a function of the distance from the grain boundary and comparing it with the bulk value in pure tungsten $d_{(111)}=0{\cdot}9137$ Å. As shown in Table 3, the (111) interplanar spacing oscillates with the distance from the grain boundary with the amplitude of oscillations gradually decreasing. Consequently by the 10–12th plane away from the grain boundary (not shown in Table 3), the oscillations are practically damped out. The results shown in Table 3 correspond to the average (111) interplanar spacings at a distance between 16·9 and 19·6 Å from the crack tip in the positive x_1 direction. It should be noted that the distance between the second and the third

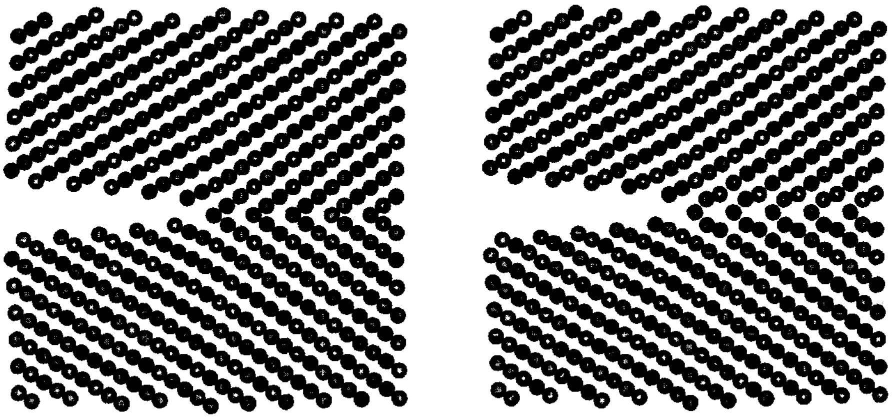

(a) (b)

Fig. 3. Initial atomic configuration of the 'clean' Σ3 (111) grain boundary in tungsten containing a crack: (a) before relaxation, and (b) after relaxation. The applied level of the stress intensity factor $K_{app} = 2{\cdot}0\,K_{Gr} = 2{\cdot}7694$ MPa m$^{1/2}$.

Table 3. The spacing, in Å, between two adjacent (111) planes as a function of the distance from the grain boundary in pure tungsten and in tungsten containing B and P grain boundary impurities

Adjacent (111) planes	*Type of grain boundary*		
	Clean	*With B*	*With P*
Above the grain boundary plane			
G.B. Plane–Plane 1	1·292	1·334	1·555
Plane 1–Plane 2	0·609	0·801	0·906
Plane 2–Plane 3	1·009	0·828	0·734
Plane 3–Plane 4	0·984	0·987	0·977
Plane 4–Plane 5	0·824	0·865	0·906
Below the grain boundary plane			
G.B. Plane–Plane 1	1·252	1·338	1·570
Plane 1–Plane 2	0·566	0·808	0·908
Plane 2–Plane 3	1·051	0·830	0·734
Plane 3–Plane 4	0·973	0·987	0·968
Plane 4–Plane 5	0·821	0·863	0·917

plane has decreased significantly relative to that in the bulk B.C.C. tungsten. This behavior is the manifestation of the crystal's tendency to reduce the free-volume of the grain boundary. It should also be noted that because the plane of the crack lies between the grain boundary plane and the first (111) plane below the grain boundary plane, the variation of the (111) interplanar spacings with the distance from the grain boundary is different for the (111) planes below and those above the grain boundary plane.

The initial atomic configuration of the Σ3 (111) grain boundary with a crack in tungsten containing boron impurity atoms located in trigonal interstitial sites and the corresponding configuration after energy minimization are shown in Fig. 4(a) and (b), respectively. The relaxed configurations for the same type of grain

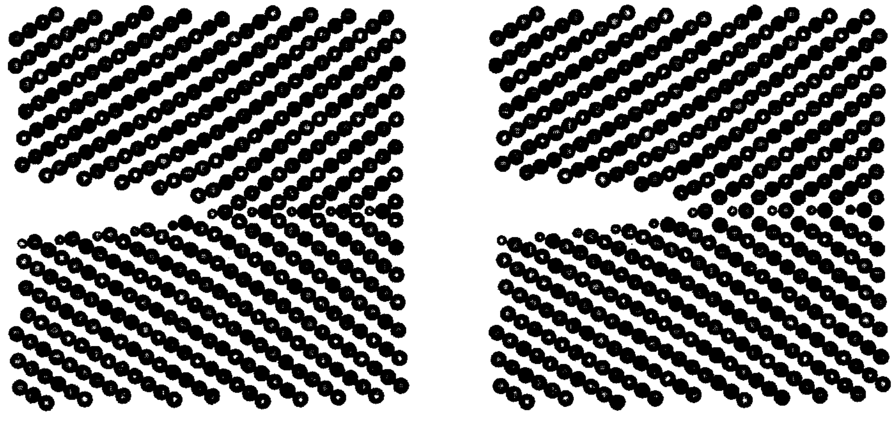

(a) (b)

Fig. 4. Initial atomic configuration of the Σ3 (111) grian boundary in tungsten containing a crack with B atoms (smaller balls) located in trigonal interstitial grain boundary sites: (a) before relaxation, and (b) after relaxation. The applied level of stress intensity factor $K_{app} = 1{\cdot}4\,K_{Gr} = 2{\cdot}9548$ MPa m$^{1/2}$.

boundary containing other grain boundary cohesion enhancers such as C and N are quite similar to the one shown in Fig. 4(b) and are not shown here for brevity. The variation of the (111) interplanar spacings with distance from the grain boundary for the relaxed configuration depicted in Fig. 4(b) is listed in Table 3. In comparison with the 'clean' grain boundary beyond the two planes adjacent to the grain boundary plane, the magnitudes of the oscillation amplitude of the (111) interplanar spacings is significantly lower. In addition, the distance of the two nearest (111) and the two next-nearest (111) planes to the grain boundary increase somewhat due to the presence of interstitial impurities of B, C or N relative to those in the case of clean grain boundary in tungsten, Table 3.

The initial atomic configuration of the $\Sigma3$ (111) grain boundary with a crack in tungsten containing phosphorus impurity atoms located in trigonal interstitial sites and the corresponding configuration after energy minimization are shown in Fig. 5(a) and (b), respectively. The relaxed configuration for the same type of grain boundary containing other grain boundary embrittlers such as S is quite similar to the one shown in Fig. 5(b) and is not shown here for brevity. The variation of the (111) interplanar spacings with distance from the grain boundary for the relaxed configuration depicted in Fig. 5(b) is listed in Table 3. In comparison with the 'clean' grain boundary, the magnitudes of the oscillation amplitude is significantly larger. Furthermore, the distance of the two nearest and the two next-nearest (111) planes from the grain boundary is significantly increased relative to those observed in the cases of the clean grain boundary and the grain boundary containing B, C or N impurities.

Material evolution at the crack tip

The progress of material evolution at the crack tip in the case of a clean $\Sigma3$ (111) grain boundary at the applied stress intensity factor $K_{app} = 2{\cdot}0\,K_{Gr} = 2{\cdot}7694$ MPa m$^{1/2}$ is shown in Fig. 6(a) and (b). This level of the applied K_I is the minimal level at which a clear evidence of crack propagation by 0·5 ps of the molecular dynamics simulation time can be obtained. A comparison of the atomic configuration after 0·5 ps simulation time, Fig. 6(a), with the original configuration, Fig. 3(a), shows a significant rearrangement of the atoms in the region surrounding the crack tip. This rearrangement leads to a significant crack blunting. No evidence of dislocation emission from the crack tip can be found. Atomic rearrangement with a small additional crack blunting continues to take place with the simulation time which can be readily established by analyzing the atomic configuration after 5 ps, Fig. 6(b). It is interesting to note that as a result of the aforementioned material evolution, a one-atom thick, one-lattice parameter-wide strip of the $(110)_{bcc}$ plane has formed at the very crack tip, Fig. 6(b). This plane is normal to the original crack plane, (111), and a [100] direction in this plane is aligned with the initial crack front-direction

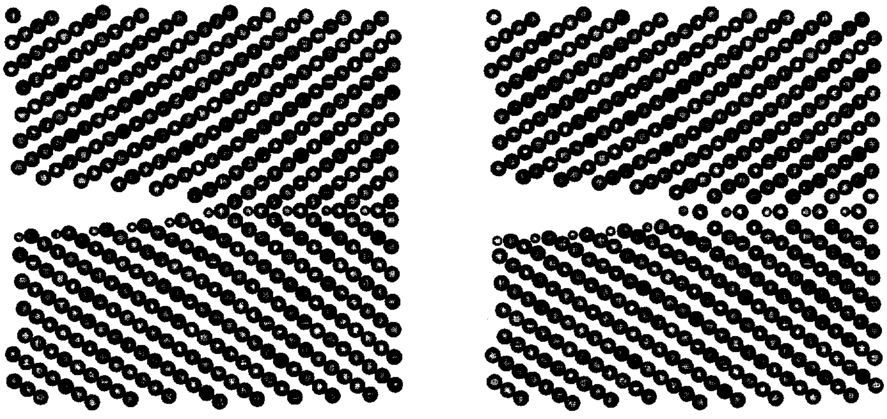
(a) (b)

Fig. 5. Initial atomic configuration of the $\Sigma3$ (111) grain boundary in tungsten containing a crack with P atoms (smaller balls) located in trigonal interstitial grain boundary sites: (a) before relaxation, and (b) after relaxation. The applied level of stress intensity factor $K_{app} = 1{\cdot}2\,K_{Gr} = 1{\cdot}4563$ MPa m$^{1/2}$.

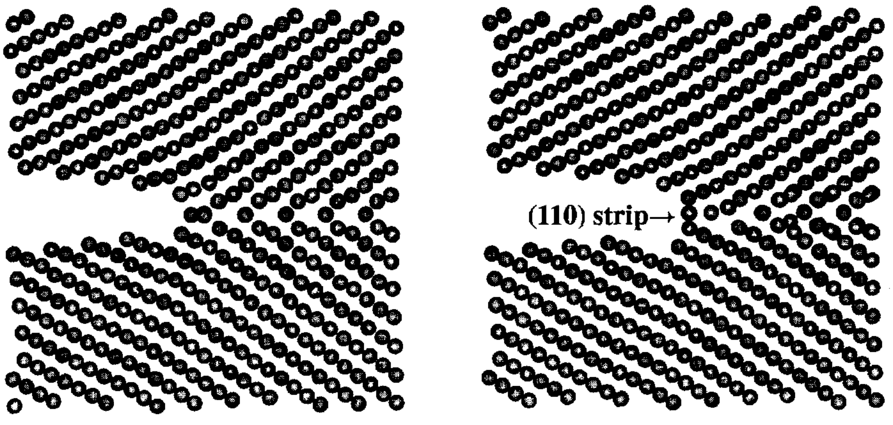

(a) (b)

Fig. 6. Atomic configuration of the Σ3 (111) 'clean' grain boundary in tungsten after the molecular dynamics simulation times: (a) 0·5 ps, and (b) 5 ps. The applied stress intensity factor $K_{\text{app}} = 2{\cdot}0\,K_{\text{Gr}} = 2{\cdot}7694$ MPa m$^{1/2}$.

$[\bar{1}10]$. The formation of this strip not only causes additional crack blunting, but also changes the local ideal work of grain boundary decohesion, which in this case can be approximated as $2\gamma_{\text{surf}}^{(100)}$, where $\gamma_{\text{surf}}^{(100)}$ is the surface energy of the (100) plane. Using the aforementioned procedure for the calculation of the surface energy, the ideal work of grain boundary decohesion has been determined as $2\gamma_{\text{surf}}^{(100)} = 0{\cdot}8128$ eV/Å^2. Since this value is higher than the one 0·2747 eV/Å^2 reported previously in Table 2, this may be the reason why crack propagation stops once the (110) strip forms at the grain boundary.

The material evolution in the region surrounding the crack tip in the cases of the Σ3 (111) grain boundary containing interstitially dissolved O, Al or S atoms is quite similar to that of the clean grain boundary and will not be discussed any further.

The progress of material evolution at the crack tip in the case of Σ3 (111) grain boundary containing interstitially dissolved B atoms at the applied stress intensity factor $K_{\text{app}} = 1{\cdot}6\,K_{\text{Gr}} = 3{\cdot}3770$ MPa m$^{1/2}$ is shown in Fig. 7(a) and (b). $K_{\text{I}} = 0{\cdot}8\,K_{\text{Gr}} = 1{\cdot}6885$ MPa m$^{1/2}$ is the minimal K_{I} value at which a noticeable crack advancement could be found by 0·5 ps of the molecular dynamics simulation time. A comparison of the atomic configuration after 0·5 ps simulation time, Fig. 7(a), with the corresponding original configuration, Fig. 4(a) shows that a significant material evolution takes place in the region surrounding the crack tip. This evolution

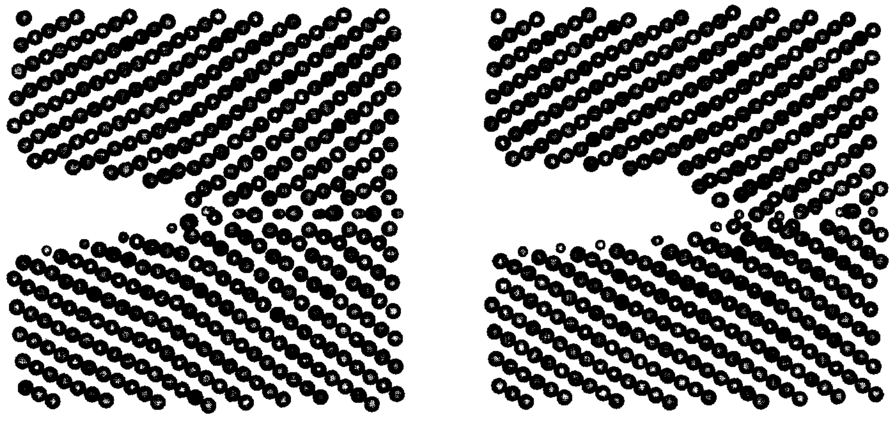

(a) (b)

Fig. 7. Atomic configuration of the Σ3 (111) 'clean' grain boundary in tungsten after the molecular dynamics simulation times: (a) 0·5 ps, and (b) 5 ps. The applied stress intensity factor $K_{\text{app}} = 2{\cdot}0\,K_{\text{Gr}} = 2{\cdot}7694$ MPa m$^{1/2}$.

gives rise to a major crack tip blunting, but no evidence of dislocation emission can be found. The aforementioned material evolution and the accompanying crack-tip blunting continues with the simulation time, Fig. 7(b). It is also important to note that after 5 ps, Fig. 7(b), B atoms form a cluster at the crack tip. This cluster is expected to enhance the intergrain bonding and, in turn, the ideal work of work of grain boundary decohesion. This may be the reason why once the cluster of B atoms is formed, the crack propagation ceases.

The progress of material evolution at the crack tip in the case of the Σ3 (111) grain boundary containing interstitially dissolved P atoms at the applied stress intensity factor $K_{app} = 1{\cdot}2\,K_{Gr} = 1{\cdot}4563$ MPa m$^{1/2}$ is shown in Fig. 8(a) and (b). $K_I = 0{\cdot}4\,K_{Gr} = 0{\cdot}4854$ M-Pa m$^{1/2}$ is the minimal value of the stress intensity factor at which a noticeable crack extension could be observed by 0·5 ps of the simulation time. A comparison of the atomic configuration after 0·5 ps of the simulation time, Fig. 8(a), with the corresponding initial configuration Fig. 5(a), shows that a significant rearrangement of the atoms takes place in the region of the grain boundary ahead of the crack. This evolution causes a significant increase in the interatomic distances in the grain boundary region. This, however, does not cause any crack tip blunting, and the crack tip remains as sharp as in the original configuration. The aforementioned material evolution continues with the simulation time and after 5 ps, Fig. 8(b), the crack tip has advanced by approximately 17 Å relative to its original position. If the simulation time is increased beyond 5 ps, the crack continues to advance until it reaches fixed atoms at the outer rim of the computational crystal.

Mechanics of grain boundary fracture

To qualify the effect of the various material evolution processes described in the previous section on the intrinsic resistance of the Σ3 (111) grain boundary in pure tungsten and in tungsten containing different impurities micro-alloying additions, the Eshelby's $\mathbf{F}_1$ conservation integral was calculated. As discussed above, $\mathbf{F}_1$ represents the force acting on the crack tip in the x_1 direction. The time evolution of this force whose initial value corresponds to the minimal level of the applied stress intensity factor at which a noticeable crack advance could be seen by 0·5 ps simulation time is given in Table 4 and plotted in Fig. 9.

In each of the cases analyzed, a positive value of $\mathbf{F}_1$ is required to initiate crack propagation. It appears that the initial values of $\mathbf{F}_1$ fall into three groups: the highest values ($\mathbf{F}_1 \approx 1{\cdot}4 \pm 0{\cdot}1$ eV/Å^2) for the Σ3 (111) grain boundary containing interstitially dissolved B, C or N atoms; the intermediate value ($\mathbf{F}_1 \approx 1{\cdot}0 \pm 0{\cdot}1$ eV/Å^2) for the clean Σ3 (111) grain boundary and the one containing dissolved O, Al or Si atoms and the lowest value ($\mathbf{F}_1 \approx 0{\cdot}7 \pm 0{\cdot}1$ eV/Å^2) for the grain boundary containing P or S impurities. These findings are

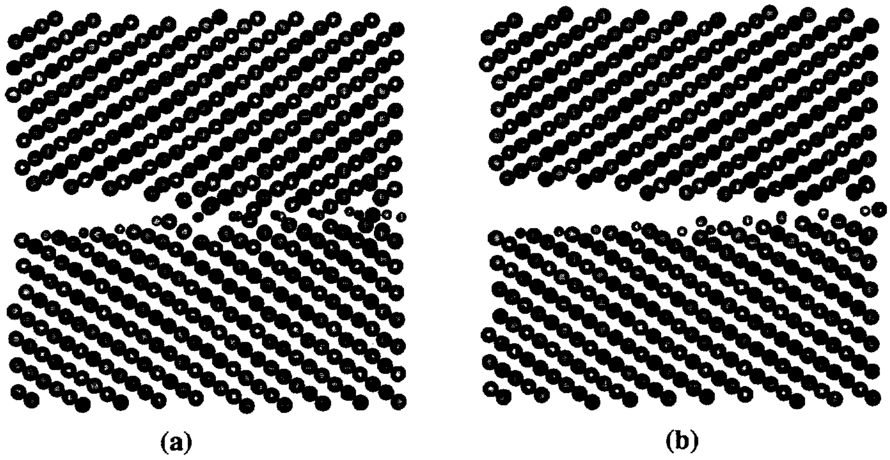
(a) (b)

Fig. 8. Atomic configuration of the Σ3 (111) grain boundary in tungsten containing phosphorus atoms (smaller balls) after the molecular dynamics simulation times of: (a) 0·5 ps, and (b) 5 ps. The applied stress intensity factor $K_{app} = 1{\cdot}2\,K_{Gr} = 1{\cdot}4563$ MPa m$^{1/2}$.

Table 4. The stress intensity factor for a reversible extension of the grain boundary crack, K_{Gr} [eqn ()12], the critical stress intensity factor for crack extension obtained during molecular dynamics simulations, K_{crit}, and the corresponding value of the Eshelby's $\mathbf{F}_1$ conservation integral

Impurity	K_{Gr}, *(MPa m$^{1/2}$)*	K_{crit}, *(MPa m$^{1/2}$)*	$\mathbf{F}_1$, *(eV/Å^2)*		
			0 ps	*0·5 ps*	*1·0 ps*
pure W	1·3847	1·6616	1·0953	0·8397	0·8256
B	2·1106	1·6885	1·4431	0·6313	0·6095
C	2·0587	1·8528	1·4006	0·6127	0·5913
N	2·0337	1·9320	1·3836	0·6053	0·5841
O	1·4781	1·4781	1·0055	0·4424	0·4269
Al	1·3900	0·5560	0·9456	0·4137	0·3952
Si	1·4795	0·5918	1·0066	0·3857	0·3722
S	1·0249	0·4100	0·6973	0·5051	0·4944
P	1·2136	0·4854	0·8257	0·6612	0·5485

fully consistent with the results for the ideal work of grain boundary decohesion listed in Table 2.

Fig. 9 further shows that as the simulation time increases the aforementioned material evoat the crack tip continues to take place and, as a result, the magnitude of the crack tip decreases. This decrease between 0 and 1 ps is significant in all the cases except for the ones involving interstitially dissolved P and S atoms at the grain boundary where the decrease in $\mathbf{F}_1$ with the simulation time is quite small. Past 1 ps no major change in the magnitude of $\mathbf{F}_1$ is found. In other words, the material evolution at the crack tip causes $\mathbf{F}_1$ to decrease but only to a lower positive value. In the cases of the clean Σ3 (111) grain boundary and such a boundary containing B, C, N, O, Al or Si, this lower level of $\mathbf{F}_1$ is not sufficient to give rise to any additional crack extension and consequently, the crack growth ceases. In sharp contrast, when the grain boundary contains P and S impurities the crack growth continues while the $\mathbf{F}_1$ remains fairly constant. The continued crack growth in the case of the grain boundary containing P and S atoms is promoted by a continued rearrangement of the grain boundary atoms which causes an increase in the interatomic distances. In other words, the atomic density in the grain boundary region continues to decrease, and in turn, lowers the cohesion strength of the grain boundary.

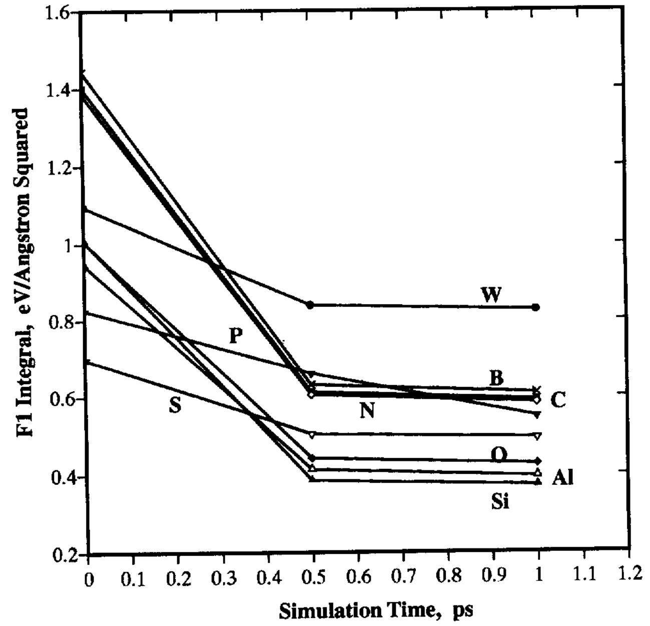

Fig. 9. Time dependence of the $\mathbf{F}_1$ integral.

In summary, the atomic simulation results obtained in the present work confirm, as has been observed experimentally, that the fracture toughness of tungsten is affected greatly by the type of impurities segregated to its grain boundaries. It should be noted, however, that in the present work only cases of clean grain boundaries and boundaries fully saturated with a single species are considered. When two or more impurity species are present Krasko[3] showed that the one whose energy at the grain boundary is lower, will preferentially segregate to the grain boundary and, thus, have the dominant effect on materials fracture toughness. In the few simulations in which partially contaminated grain boundaries, that is the grain boundary was not fully saturated with impurities, were used, we observed that the character of the effect (embrittling or cohesion enhancing) ddi not change but its magnitude was lower.

It should be noted that our results differ somewhat from the findings of Krasko.[3] Specifically, N was identified by Krasko[3] as a grain boundary embrittler while in the present work this element was found to be a cohesion enhancer. Furthermore, O, Al and Si were identified by Krasko[3] as grain boundary embrittlers while these elements were found to be neutral in the present work. As far as H is concerned, the embedded energy fucntions for this element were not available and its effect on grain boundary cohesion could not be studied. We believe that the differences between the results obtained by Krasko[3] and our results stem from the differences in the simulation methods used, Krasko[3] applied molecular statics and constrained the motion of atoms to the planes parallel to the grain boundary. This constraint was lifted in the present work, and the simulations were carried out using molecular dynamics. This method allows the atoms to relax into the configuration associated with a lower energy and is generally considered as a more appropriate simulation method for non-zero temperatures.

CONCLUSION

Based on the results obtained in the present work, the following main conclusions can be drawn:

(1) with respect to their effect on the intrinsic fracture resistance of the $\Sigma3$ (111) grain boundary in tungsten, the atomic species analyzed can be divided into three groups:

(2) Interstitially dissolved B, C and N are strong grain boundary cohesion strengtheners which both enhance intergrain bonding and give rise to a lower level of effective loading at the crack tip by promoting crack tip blunting. There is some evidence that clustering of the interstitial atoms is, at least partly, responsible for the observed fracture resistance.

(3) O, Al and Si do not significantly affect either the ideal work of grain boundary decohesion or the crack blunting processes relative to those observed in the case of the clean $\Sigma3$ (111) grain boundary.

(4) P and S are strong grain boundary embrittlers which both significantly lower the ideal work of grain boundary decohesion and impede with crack tip blunting processes.

(5) Regardless whether the intrinsic fracture of the $\Sigma3$ (111) grain boundary is measured using the ideal work of grain boundary decohesion or by the critical value of the $\mathbf{F}_1$ integral, removal of deleterious impurities such as P or S, by either material purification or by the site competition effect with B, C or N can have a great potential in achieving the goal of producing the 'ductile' tungsten.

ACKNOWLEDGEMENTS

The work was supported by the US Army Research Office, Grant DAAH04-96-1-0917 and by the National Science Foundation under Grants DMR-9317804 and CMS-9531930. The authors are indebted to Dr Wilbur C. Simmons of ARO and to Drs Bruce MacDonald and William A. Spitzig of NSF for the continuing interest in the present work. Helpful discussions with Mr Shugang Lai are greatly appreciated.

REFERENCES

1. Dowding, R. J., Tungsten heavy alloys: a tutorial review. *Powder Metallurgy in Aerospace and Defense Technologies*, Vol. 2, MPIF, Princeton, NJ, 1991.
2. Magness, L. S. & Farrand, T. G., *Proceedings of the 1990 Army Science Conference*, pp. 465–79.
3. Krasko, G. L., *Int. J. Refractory Metals and Hard Materials*, 1994, **12**, 251.
4. Briant, C. L. and Banerji, S. K., *Embrittlement of Engineering Alloys*, Academic Press, New York, 1983, p. 21.
5. Mescall, J. F. & Rogers, H., *Innovations of Ultra-high Strength Steel Technology*, ed. G. B. Olson, M. Azrin & E. S. Wright. 34th Sagamore Army Materials Research Conference, August 30–September 3, 1987, Lake George, NY, pp. 287–314.
6. Guttmann, M. & McLean, D., *Interfacial Segregations*, ASM, Metals Park, OH, 1979, p. 261.
7. Wukusick, C., *Refractory Metals and Alloys IV — Research and Development.* Gordon and Breach, New York, 1967, pp. 231–45.
8. Booth, J. G., Jaffee, R. I. & Salkovitz, E. I., *Metals for the Space Age.* Reutte, Austraia, 1965, pp. 547–70.
9. Povarova K. B. *et al.*, Effect of microalloying on the low-temperature plasticity and technological expediency of vacuum-melted tungsten of technical purity. *Izvestiya Acad. Nauk SSSR. Metalli*, 1990, **1**, 76–81 (translation: *Russian Metallurgy, Metally*, 1990, **1**, 74–9).

10. Povarova, K. B. *et al.*, Effect of microalloying on the ductile–brittle transition temperature of tungsten. *Izvestiya Acad. Nauk SSSR. Metalli*, 1987, **1**, 134–41 (translation: *Russian Metallurgy, Metally*, 1987, **1**, 129–36).
11. Tolstobrov, Yu. O. and Povarova, K. B., Effect of micro-alloying with boron on the structure and properties of tungsten. *Fizika i Khimiya Obrabotki Materialov*, 1987, **21**, 121 (in Russian).
12. Daw, M. S. & Baskes, M. I., *Phys. Rev.*, 1984, **B29**, 6443.
13. Daw, M. S. & Baskes, M. I., *Phys. Rev. Lett.*, 1983, **50**, 1285.
14. Foiles, S. M., Baskes, M. I. & Daw, M. S., *Phys. Rev.*, 1986, **B33**, 7983.
15. Finnis, M. W. & Sinclair, J. E., *Philosophical Magazine A.*, 1984, **50**, 45.
16. Sih, G. C. & Liebowitz, H., *Fracture — An Advanced Treatise*, Vol. II. Academic Press, New York, 1968, p. 67.
17. Eshelby, J. D., *J. Elasticity*, 1975, **5**, 321.
18. Hoagland, R. G., Daw, M. S. & Hirth, J. P., *J. Mater. Res.*, 1991, **6**, 2565.
19. Gerald, C. F. & Wheatley, P. O., *Applied Numerical Analysis*, 5th edn, Addison-Wesley Publishing Company Inc., Reading, MA, 1994, p. 221.
20. McMeeking, R. M., *J. Mech. Phys. Solids*, 1977, **25**, 357.
21. Fletcher, R. & Reeves, C. M., *Comput. J.*, 1964, **7**, 149.